

## More Frequent Sudden Stratospheric Warming Events due to Enhanced MJO Forcing Expected in a Warmer Climate

WANYING KANG

*School of Engineering and Applied Sciences, Harvard University, Cambridge, Massachusetts*

ELI TZIPERMAN

*Department of Earth and Planetary Sciences, and School of Engineering and Applied Sciences, Harvard University, Cambridge, Massachusetts*

(Manuscript received 24 January 2017, in final form 21 July 2017)

### ABSTRACT

Sudden stratospheric warming (SSW) events influence the Arctic Oscillation and midlatitude extreme weather. Observations show SSW events to be correlated with certain phases of the Madden-Julian oscillation (MJO), but the effect of the MJO on SSW frequency is unknown, and the teleconnection mechanism, its planetary wave propagation path, and time scale are still not completely understood. The Arctic stratosphere response to increased MJO forcing expected in a warmer climate using two models is studied: the comprehensive Whole Atmosphere Community Climate Model and an idealized dry dynamical core with and without MJO-like forcing. It is shown that the frequency of SSW events increases significantly in response to stronger MJO forcing, also affecting the averaged polar cap temperature. Two teleconnection mechanisms are identified: a direct propagation of MJO-forced transient waves to the Arctic stratosphere and a nonlinear enhancement of stationary waves by the MJO-forced transient waves. The MJO-forced waves propagate poleward in the lower stratosphere and upper troposphere and then upward. The cleaner results of the idealized model allow identifying the propagating signal and suggest a horizontal propagation time scale of 10–20 days, followed by additional time for upward propagation within the Arctic stratosphere, although there are significant uncertainties involved. Given that the MJO is predicted to be stronger in a warmer climate, these results suggest that SSW events may become more frequent, with possible implications on tropospheric high-latitude weather. However, the effect of an actual warming scenario on SSW frequency involves additional effects besides a strengthening of the MJO, requiring further investigation.

### 1. Introduction

Major sudden stratospheric warming (SSW) events occur in the Arctic stratosphere at a frequency of about six events per decade and involve a reversal of the stratospheric vortex, accompanied by a steep rise of the polar cap temperature (Craig et al. 1959; Limpasuvan et al. 2004). SSW events affect, within weeks to months, the tropospheric jet, the Arctic Oscillation, midlatitude blocking systems, and extreme weather events (Baldwin and Dunkerton 1999; Gerber and Polvani 2009; Harnik and Lindzen 2001; Thompson et al. 2002; Cohen et al. 2007; Kolstad et al. 2010). The long time scale of downward propagation of stratospheric signals (Cohen et al. 2007; Kushner and

Polvani 2004) and the potential teleconnection with the tropical variability modes (e.g., MJO, Garfinkel et al. 2012a) may extend the predictability of these systems. In global warming scenarios, some general circulation model (GCM) studies find an increased frequency of SSW events (Schimanke et al. 2013; Bellet al. 2010; Charlton-Perez et al. 2008), but these results are not conclusive (Butchart et al. 2000; McLandress and Shepherd 2009; Mitchell et al. 2012), requiring a deeper understanding on the mechanisms involved and the role of different forcing factors.

The triggering of SSW events involves upward-propagating planetary waves (Matsuno 1971; Limpasuvan et al. 2004), which were shown to be related to tropospheric sea level pressure patterns, October Eurasian snow cover, sea surface temperature, and more (Hardiman et al. 2008; Garfinkel and Hartmann 2008; Garfinkel et al. 2010; Hurwitz et al. 2012). The Arctic stratosphere, and

---

*Corresponding author:* Wanying Kang, wanyingkang@g.harvard.edu

SSW events in particular, are known to be affected by tropical variability as well, including the quasi-biennial oscillation (Holton and Tan 1980; Garfinkel et al. 2012b) and the Madden–Julian oscillation (MJO) (Garfinkel et al. 2012a).

Our concern here is the teleconnection between the MJO (Madden and Julian 1971; Zhang 2005) and SSW events. The MJO, an eastward-propagating tropospheric convection center in the equatorial Indian Ocean and Pacific sectors, is the dominant intraseasonal tropical variability mode. Recent work demonstrated that it affects the polar stratospheric vortex (PSV) and SSW events using both reanalysis data and an atmospheric model (Liu et al. 2014; Garfinkel et al. 2012a, 2014). Polar vortex weakening was also shown to be related to tropical convection in observations by Goss et al. (2016).

The MJO, with its dominant zonal wavenumbers of 1 or 2 (Wheeler and Kiladis 1999), efficiently excites planetary waves that propagate to higher latitudes (Karoly and Hoskins 1982). It was shown in reanalysis data and models to be related to high-latitude tropospheric variability, including Northern Hemisphere blocking, stronger upward Eliassen–Palm (EP) flux in the midlatitudes, the Pacific–North American pattern, and a warmer Arctic surface (Yoo et al. 2012b, 2014, 2012a; Cassou 2008). Both observations (Slingo et al. 1999; Hendon et al. 1999; Jones and Carvalho 2006; Oliver and Thompson 2012) and models (Lee 1999; Caballero and Huber 2010; Schubert et al. 2013; Arnold et al. 2013, 2014) indicate that MJO activity is expected to strengthen in a warmer climate.

While most GCMs have difficulties simulating the MJO, a previous study (Arnold et al. 2014), using the superparameterized Community Earth System Model (SP-CESM), which produces a fairly realistic MJO simulation, showed that the MJO is expected to strengthen under a higher CO<sub>2</sub> scenario and showed the mechanism to be due to the steepening of the moist static energy profile in a warmer climate. The same study also noted a warmer Arctic stratosphere during winter and speculated that this may be related to MJO-related wave fluxes. Our main result here is that the frequency of SSW events increases, the Arctic stratosphere warms, and the polar night jet weakens as a result of stronger MJO forcing, consistent with and explaining the findings of Arnold et al. (2014).

We are also concerned here with three specific questions regarding the MJO–SSW teleconnection. The first is the time scale of the teleconnection. Garfinkel et al. (2012a) showed a warming of the polar vortex 10 days after MJO phase 7 and another one about a month after MJO phases 2 and 3, leaving the teleconnection time

somewhat uncertain. Because the MJO is quasi periodic, an observed connection seen after a given MJO phase may be either a slow response to earlier phases or a faster response to later phases. To reduce the ambiguity in the teleconnection time scale, it is useful to understand the physical processes involved. We analyze the teleconnection time scale for this path, starting with a horizontal propagation from the tropics and followed by additional time for vertical propagation within the Arctic stratosphere, although we also note some caveats that may affect the specific time scales deduced. The second issue of interest here is the teleconnection path. Garfinkel et al. (2014) showed evidence that, through constructive interference with climatological stationary waves, the perturbation associated with MJO phase 7 (3) leads to an in-phase strengthening (out-of-phase weakening) of the eddy meridional heat flux, but they did not discuss the path of propagation. We show that there is an MJO-forced wave train propagating poleward and upward through the upper troposphere and lower stratosphere to the Arctic stratosphere, which is consistent with the abovementioned teleconnection time. The third specific issue examined here involves the way the MJO waves affect SSW events. We demonstrate two different mechanisms in which the MJO-forced transient waves affect SSW events, both distinct from the constructive interference discussed by Garfinkel et al. (2014): via a direct propagation of these transient waves and a corresponding EP flux into the polar cap and, distinctly, via a nonlinear interaction with the climatology that changes the stationary wave forcing.

To address these issues, we use both an idealized atmospheric model based on the Community Atmospheric Model (Neale et al. 2010), with and without the artificial wavenumber 1 ( $k = 1$ ) MJO forcing, and the comprehensive Whole Atmosphere Community Climate Model (WACCM; Marsh et al. 2013) with and without enhanced convective entrainment rate to strengthen the MJO variability. The two models complement each other, providing both simplicity of analysis and realism; the idealized model enables a clean diagnosis of teleconnection propagation signals, and WACCM adds to the relevance of the idealized model results.

In the following section we present the two models used, the MJO forcing structure added to the idealized model, and the modification of convection coefficients used to enhance the MJO signal in WACCM in order to study the Arctic stratospheric response. While WACCM simulates a too-weak MJO like most GCMs, the adjusted convection coefficients strengthen the MJO signal, although this affects the realism of other aspects of

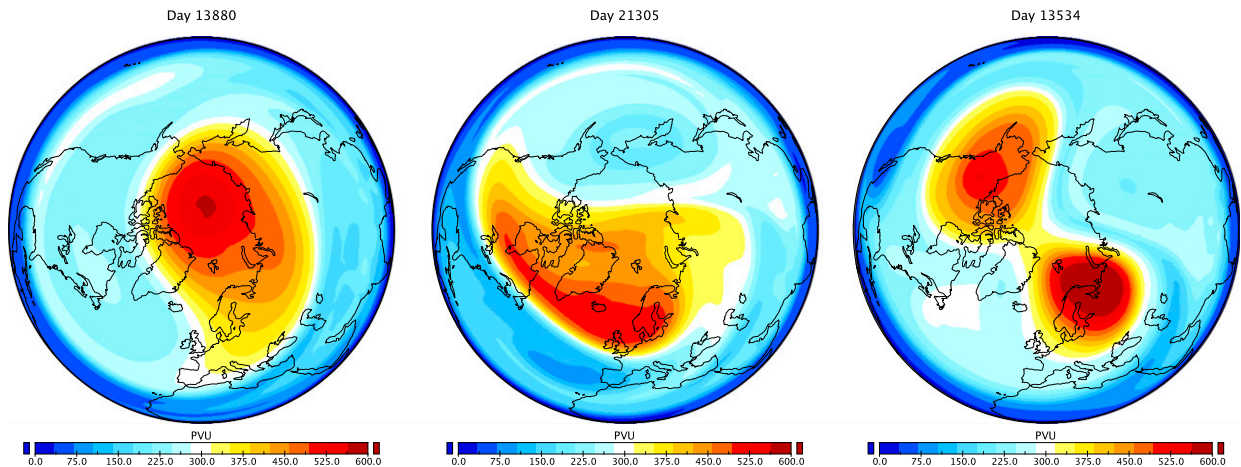


FIG. 1. Examples of SSW events in the control, unforced, idealized model experiment, showing snapshots of Ertel PV (PVU): (left) a normal polar vortex at 10 mb, (center) a “displacement” event, and (right) a “split” SSW event.

the model. Yet WACCM still provides a more realistic check on our results than is possible with the idealized GCM. We then present the results (section 3), showing the increased SSW frequency in both models, analyze the heat budget of the Arctic stratosphere with and without the MJO forcing, show evidence for the propagation of MJO-forced transient waves to the Arctic stratosphere, and analyze the stationary wave response affecting the Arctic stratosphere. We provide conclusions in section 4.

## 2. Methods

### a. Idealized model configuration

The idealized model experiments are configured based on the idealized physics component set in the Community Earth System Model (CESM), version 1.2.2 (Neale et al. 2010), which follows Held and Suarez (1994). Radiation and convection are replaced by a restoring term to an equilibrium temperature with a time scale of 40 days everywhere except near the surface, where friction is represented by restoring the horizontal wind to zero strongly (the restoring time scale decreases gradually from 40 to 4 days below 700 mb; 1 mb = 1 hPa). The finite-volume core is used, and the horizontal resolution is  $1.875^\circ$  in latitude and  $2.5^\circ$  in longitude, with 30 pressure–sigma hybrid layers from the surface to 1.67 mb. To avoid numerical instability caused by wave reflection at the model top, we add a weak damping to the top three layers, restoring the wind to climatology with a time scale that is linearly reduced from 40 to 15 days. The background state for the prognostic variables of zonal wind  $U$ , meridional wind  $V$ , and temperature  $T$  is set to the winter (DJF) climatology of  $1 \times \text{CO}_2$  SP-CESM in the study of Arnold

et al. (2014) using the method of Hall (2000), by calculating appropriate forcing terms for the temperature and momentum equations, in addition to restoring the temperature to the climatology of Arnold et al. (2014). While our vertical resolution in the stratosphere, as that of closely related studies (Garfinkel et al. 2014), may not be optimal for studying SSW events (Richter et al. 2014), Fig. 1 shows example SSW events in the unforced idealized model run, demonstrating the model skill in representing these events. We complement this model with the more realistic WACCM experiments described below, reinforcing the relevance of the idealized model analysis.

### b. MJO forcing

MJO forcing is added to the idealized model as an external heating source, with a zonal wavenumber 1 structure, a period of  $2\pi/\omega = 40$  days, and a maximum heating rate of  $5 \text{ K day}^{-1}$ . This forcing is only applied over a longitudinal window from  $60^\circ\text{E}$  to  $180^\circ$ , so that the adiabatic heating structure is given by

$$H = A \exp\left(-\frac{\sin^2\phi}{2\sigma_y^2}\right) \sin(k\lambda - \omega t) \cos\left[\frac{\log(p_0/p)}{\log(p_{\text{surf}}/p_0)} \frac{\pi}{2}\right] \times W(\lambda), \quad (1)$$

where  $W(\lambda)$  is the longitudinal window,  $\phi$  is latitude,  $\sigma_y = 5^\circ$ ,  $k$  is the forcing zonal wavenumber,  $\omega$  is the forcing frequency,  $p$  is pressure,  $p_0$  is tropopause pressure (100 mb),  $p_{\text{surf}}$  is the surface pressure (1000 mb), and  $A$  is the heating amplitude. The perfectly periodic nature of this forcing, unlike that of the observed MJO, makes it easier below to diagnose the teleconnection

path and time scale. We define phase 1 of the idealized MJO forcing to correspond to the time in which the heating center is at 90°E.

### c. SC-WACCM

The Whole Atmosphere Community Climate Model (Marsh et al. 2013) is a high-top GCM, with 66 layers extending to the thermosphere and with convection and front-induced gravity wave drag parameterization, which were found important for a realistic SSW simulation (Richter et al. 2014). We use the “specified chemistry” version of WACCM (SC-WACCM), which was verified to be consistent with the full WACCM and with observations (Smith et al. 2014).

The CAM-based WACCM, like most atmospheric general circulation models, underestimates the MJO strength (Inness et al. 2003; Zhang et al. 2006; Subramanian et al. 2011). It is known that a stronger MJO may be obtained by adjusting convection parameters, in particular increasing the entrainment rate (Neale et al. 2010; Klein et al. 2012; Benedict et al. 2013), and we use a doubled entrainment rate for our enhanced MJO forcing experiments with WACCM. Arnold et al. (2014) found that the standard deviation of daily equatorial (10°S–10°N) precipitation within the MJO band (defined as 20–100 days, corresponding to zonal wavenumbers 1–3) responds to the quadrupling of CO<sub>2</sub> by increasing from 0.69 to 1.24 mm day<sup>-1</sup> in SP-CESM. WACCM shows a corresponding increase from 0.62 to 0.73 mm day<sup>-1</sup> when the entrainment rate is doubled. Comparing the modified entrainment rate run with the standard run allows us to extract the response to the MJO forcing, similar to the comparison of the forced and unforced idealized runs. The modification to the entrainment rate has additional, possibly undesired, effects on the mean state (e.g., Benedict et al. 2013). Our comparative analysis of both WACCM and the idealized model provides some assurance that the enhanced MJO forcing is indeed responsible for the SSW response we observe in WACCM.

## 3. Results

We now present and analyze the results of the MJO-forced runs, compared to the control runs. We first (section 3a) show that the number of SSW events increases as a result of MJO forcing in both models and that there is a connection between the MJO and polar cap temperature in the models used, similar to the one seen in reanalysis by Garfinkel et al. (2012a). We then (section 3b) show that MJO-forced transient waves start propagating from the tropics at around MJO phase 5, reaching the lower Arctic stratosphere and then

vertically propagating within the Arctic stratosphere. We analyze the EP flux resulting from these waves and their possible direct effect on SSW events. Finally (section 3c), we find that the MJO forcing also modifies the climatology and therefore changes the stationary waves seen by the polar cap, which also contributes to the change in SSW frequency.

### a. SSW response to MJO forcing

Figure 2a shows time series of the zonal mean  $U$  at 70°N and 10 mb for the idealized perpetual winter simulations, showing both the unforced control run (blue) and the run with MJO forcing (red); Fig. 2b is the corresponding plot for WACCM, showing  $U$  at 60°N. SSW events are marked by small triangles along the time axis. The statistics of SSW events are summarized in Table 1 using several criteria for SSW events, based on the zonal mean  $U$  at 60°, 65°, and 70°N, and using different thresholds (0 and 5 m s<sup>-1</sup>). The reversal of the  $U$  averaged over the polar cap (>60°N) has been used as a criterion for SSW events, but the reversal of the zonal mean  $U$  at 60°N has been used more recently (Butler et al. 2015). Butler et al. (2015) noted that more frequent SSW events are diagnosed when using the reversal of wind at higher latitudes as the criteria, which is also what we found in the idealized model (and in WACCM, although it is not as sensitive as the idealized model to the latitude used). The SSW simulation in the idealized model is not completely realistic, and as a result its SSW frequency is too low when using  $U$  at 60°N as the criteria; we therefore plot the 70°N wind instead (Fig. 2a). After adding MJO forcing, the frequency of SSW events is nearly doubled using all these criteria (except for the most restrictive criteria for the idealized model) in both the idealized model and WACCM (Table 1).

Figure 3 shows the time and zonally averaged difference temperature and zonal velocity between the forced and unforced runs of both models, as a function of latitude and pressure. A warming and weakening of the polar night jet in the Arctic stratosphere is clearly seen, mostly reflecting a change to the SSW frequency, as the climatology during times with no SSW events changes only to a smaller degree (not shown). The 95% significance level is indicated by shading, using the Student's  $t$  test and setting the number of degrees of freedom to the number of years used. While a link between the MJO and SSW events has been analyzed previously (Garfinkel et al. 2012a, 2014), the change in SSW frequency resulting from increased MJO forcing is our main novel result here. Given the expected stronger MJO in warm past and future climates (e.g., Arnold et al. 2014), this resulting change to SSW frequency is

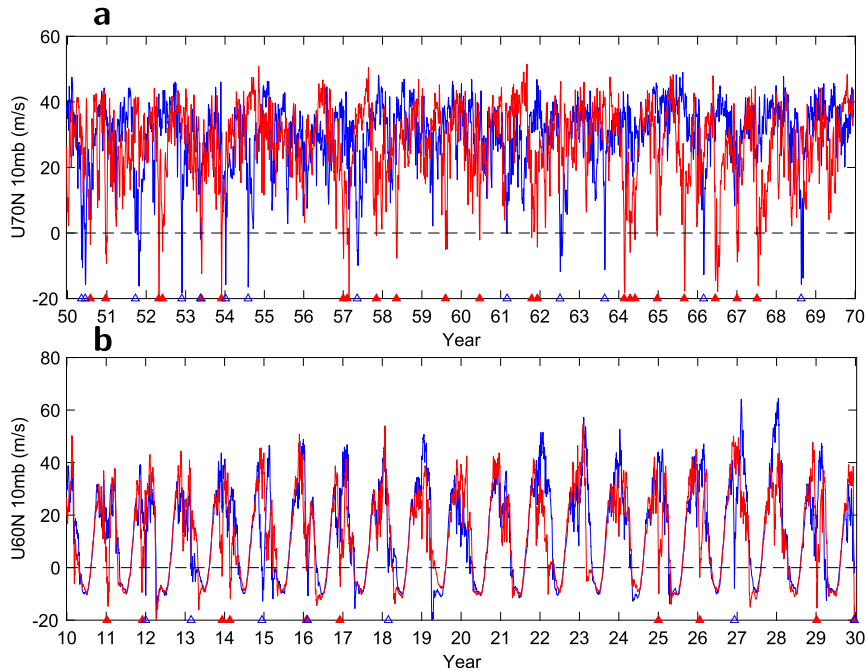


FIG. 2. Time series of (a) zonal mean zonal wind at 70°N and 10 mb ( $\text{m s}^{-1}$ ) for the idealized model and (b) zonal mean zonal wind at 60°N and 10 mb ( $\text{m s}^{-1}$ ) for WACCM. Control experiment in blue and MJO-forced experiment in red. SSW events are marked by triangles on the  $x$  axis. See text for details of SSW definition used.

interesting, and we next attempt to investigate the teleconnection mechanism.

We begin by considering the heat budget of the region 20–70 mb and 65°–85°N for the forced and unforced runs of both models (Figs. 4a,b). We denote zonal averages by  $\langle f \rangle$  and time averages by  $\bar{f}$ ; the deviation from a time average is denoted with a prime,  $f - \bar{f} = f'$ ; and the deviation from zonal mean is indicated by an asterisk,  $f - \langle f \rangle = f^*$ . The difference between the forced and unforced runs (yellow bars) shows that the main reason for the temperature

increase is an enhanced meridional heat flux by stationary waves  $\langle \bar{V}^* \bar{T}^* \rangle$  in both the idealized model (Fig. 4a) and WACCM (Fig. 4b). Since the sum over all budget terms must vanish for each run (forced and unforced) and therefore also for their difference, the increased heating rate due to stationary waves must be accompanied by a decrease in another term. In the idealized model this is achieved by the vertical advection by the zonal mean circulation  $\langle \bar{\omega} \rangle \langle \bar{T}_p \rangle$  (Fig. 4a), while in WACCM the compensation is by a decrease in the meridional heat flux by transient waves (Fig. 4b).

TABLE 1. SSW event counts with and without MJO forcing as defined in section 2. An SSW event is diagnosed when the zonal average zonal wind becomes easterly at 10 mb and varying latitudes and drops below the criteria of 0 or 5  $\text{m s}^{-1}$ . No new event is counted unless the wind is back to normal (above the criteria) for at least 20 days. WACCM experiments were run for 30 years with an annual cycle, and the idealized dry core experiments were run for 50 years with perpetual winter (DJF) climatology. When diagnosing SSW events, we searched for the first day when the zonal mean 10-mb wind in a corresponding latitude drops below the threshold after at least 20 continuous days of being above the threshold. The results were not sensitive to changing the criterion from 10 to 50 days. The final warming events in WACCM were excluded by restricting the events to DJF.

	60°N		65°N		70°N	
	$U = 0 \text{ m s}^{-1}$	$U = 5 \text{ m s}^{-1}$	$U = 0 \text{ m s}^{-1}$	$U = 5 \text{ m s}^{-1}$	$U = 0 \text{ m s}^{-1}$	$U = 5 \text{ m s}^{-1}$
Ideal control	9	9	24	24	30	34
Ideal MJO = 5 $\text{K day}^{-1}$	10	34	37	57	59	80
WACCM control	8	8	10	10	13	13
WACCM MJO enhanced	14	16	16	21	20	24

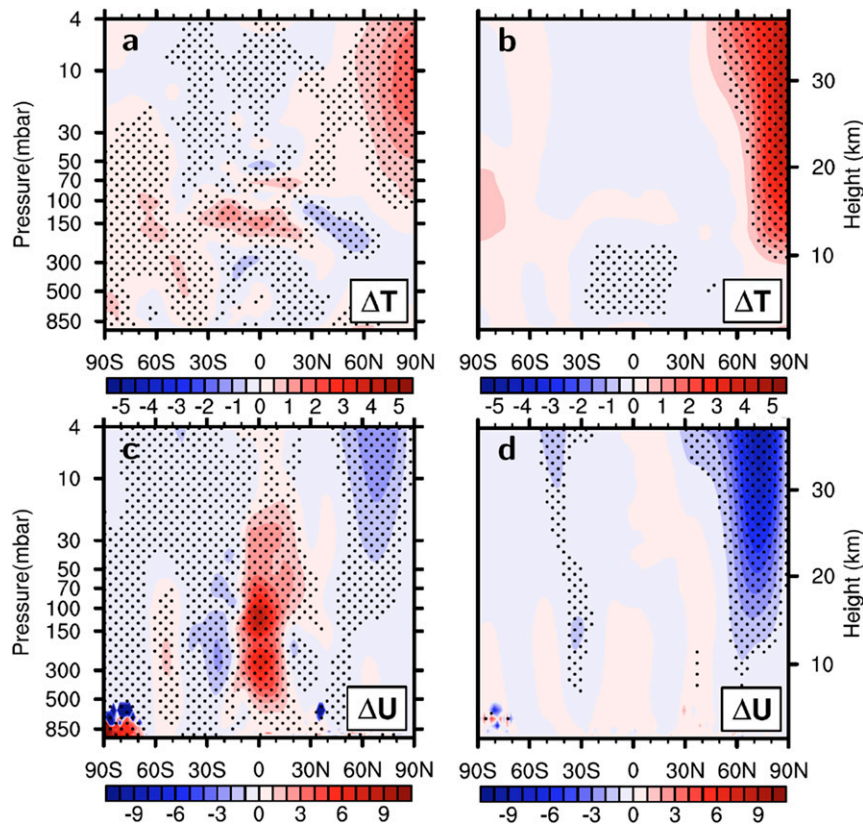


FIG. 3. Changes in climatology (top) zonal mean temperature ( $^{\circ}\text{C}$ ) and (bottom) zonal wind ( $\text{m s}^{-1}$ ) in response to MJO forcing in (a),(c) the idealized model and (b),(d) SC-WACCM. Stippled areas are 95% significant with the Student's  $t$  test.

The enhancement of stationary eddy heat transport ( $\overline{\mathbf{V}^*T_y^*}$ ) is significant in both models (section 3c), while the total heat flux due to transient waves does not increase significantly. We decompose the total EP flux into four categories in Fig. 5: transient waves in the MJO frequency range (35–45 days in the idealized model and 20–100 days in WACCM), higher-frequency waves, and lower-frequency waves (including stationary waves). The stationary upward EP flux is enhanced by the MJO forcing, as seen in the temperature budget (Fig. 4). The vertical EP flux at the MJO frequency is also significantly enhanced, while the contribution of higher frequencies is reduced. The constructive interference between transient waves and climatological stationary waves may lead to enhanced warming during warm events (and to cooling at other times) and help trigger SSW events as discussed by Garfinkel et al. (2014), but it will vanish under time averaging and therefore cannot contribute to the Arctic warming in our analysis.

Next, to demonstrate that the added MJO forcing affects the polar Arctic, we follow Garfinkel et al. (2012a) and plot in Fig. 6 a composite of the polar cap

temperature ( $65^{\circ}$ – $90^{\circ}\text{N}$  and 10 mb) as a function of the MJO phases (defined following Wheeler and Hendon 2004). The diagonally banded signal shows a clear relation between the MJO phase and the Arctic polar cap temperature in both models. Since the MJO forcing in the idealized model is perfectly periodic and this model has no seasonal cycle, the correlation is uniformly strong for all MJO phases. WACCM, with its seasonal cycle and nonperiodic MJO, does show stronger correlation for MJO phases 2, 3, and 5, which matches the findings of Garfinkel et al. (2012a) in reanalysis remarkably well. The difference in polar cap temperature between different phases of the MJO is about 6 K, indicating a strong role of the MJO. The response to increased MJO forcing in WACCM is surprisingly strong, given that the MJO strengthening is less than 20% using the measures shown in section 2c. We cannot rule out the possibility that the change in entrainment rate leads to effects other than strengthening of the MJO, which also affect the SSW frequency. However, this diagram cannot unambiguously show which MJO phase initiates the teleconnection, and further

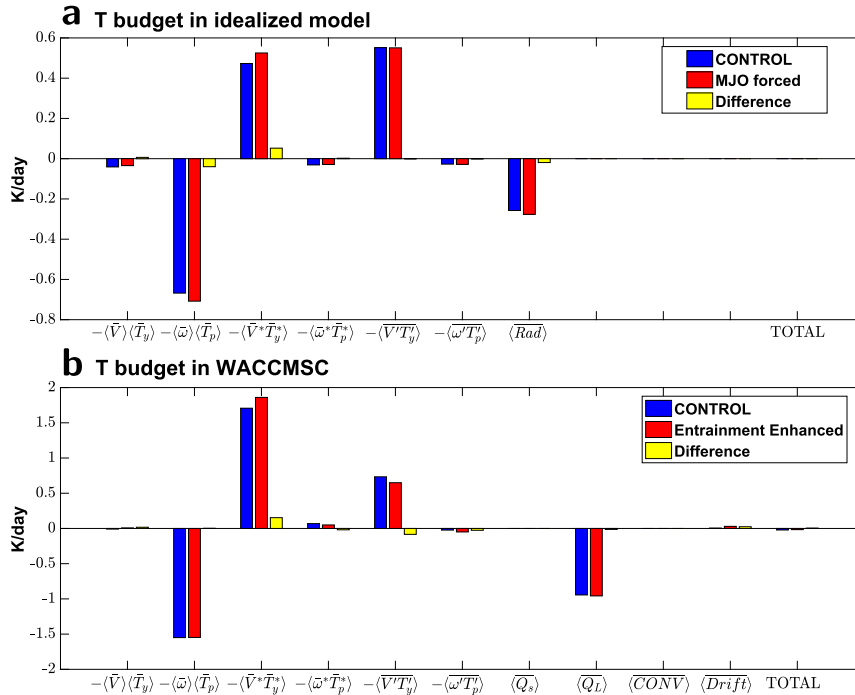


FIG. 4. Terms in the temperature budget ( $\text{K day}^{-1}$ ) in the region  $65^{\circ}$ – $85^{\circ}\text{N}$  and 20–70 mb, for (a) the idealized model and (b) WACCM. From left to right, the terms are 1) horizontal advection by zonal and time mean circulation, 2) vertical advection by zonal and time mean circulation, 3) horizontal transport by stationary waves, 4) vertical transport by stationary waves, 5) horizontal transport by transient waves, 6) vertical transport by transient waves, 7) diabatic heating rate ( $\overline{\text{Rad}}$ ) for the idealized model in (a) and shortwave heating rate ( $\langle Q_s \rangle$ ) for WACCM in (b), 8) longwave heating rate in (b) only, 9) convective heating rate in (b) only, 10) temperature drift in (b) only, and 11) sum of all terms (its small value verifies that the budget is consistently calculated).

investigation on the teleconnection path and time scale are presented in the next section.

### b. Teleconnection mechanism: Propagation of transient MJO-forced waves

One expects the teleconnection mechanism to involve planetary waves. To show the phase propagation first, we consider in Figs. 7a,b the zonal wavenumber 1 contribution to Ertel PV Hovmöller composites for the forced idealized model, calculated by averaging the PV anomaly (forced response minus unforced climatology) over all occurrences of a given MJO phase. The purpose of these composites is to identify and analyze the propagation of the MJO signal from the tropical troposphere to the Arctic stratosphere. Shaded areas in these plots indicate 95% statistical significance in Figs. 7a,b and 90% in Fig. 7c, based on the Student's  $t$  test, where the number of degrees of freedom was calculated based on the number of separate MJO phase events following Garfinkel et al. (2012a). Since the  $k = 1$  structure vanishes under zonal average, we average over the longitude range  $90^{\circ}\text{E}$ – $180^{\circ}$  where the

propagation takes place (Fig. 8, top). The perturbation initiated in the tropics at MJO phases 3–5 arrives at  $60^{\circ}$ – $80^{\circ}\text{N}$  by phases 7 and 8 of the next MJO cycle, corresponding to about 60 days of phase propagation time scale (i.e., about one and a half MJO cycles). Figure 7b shows that once at high latitudes, the signal propagates up from 70 to 20 mb from MJO phases 7 and 8 to phases 2 and 3 in the next cycle, corresponding to about 10–15 more days.

However, given that the group velocity is a more relevant measure of energy propagation, Fig. 7c shows the similar composite of the northward pseudomomentum flux, which should propagate at the group velocity speed [we follow the definition in Takaya and Nakamura (2001), formulated in spherical and pressure coordinates, as shown in the appendix]. Positive pseudomomentum flux anomalies start in the tropics during phases 3 and 4 and phases 5 and 6, shown in Fig. 7c by two red patches near the equator, indicating northward propagation (note that tick marks indicate the middle of MJO phases). These positive anomalies may be linked to the positive anomaly that later appears to propagate

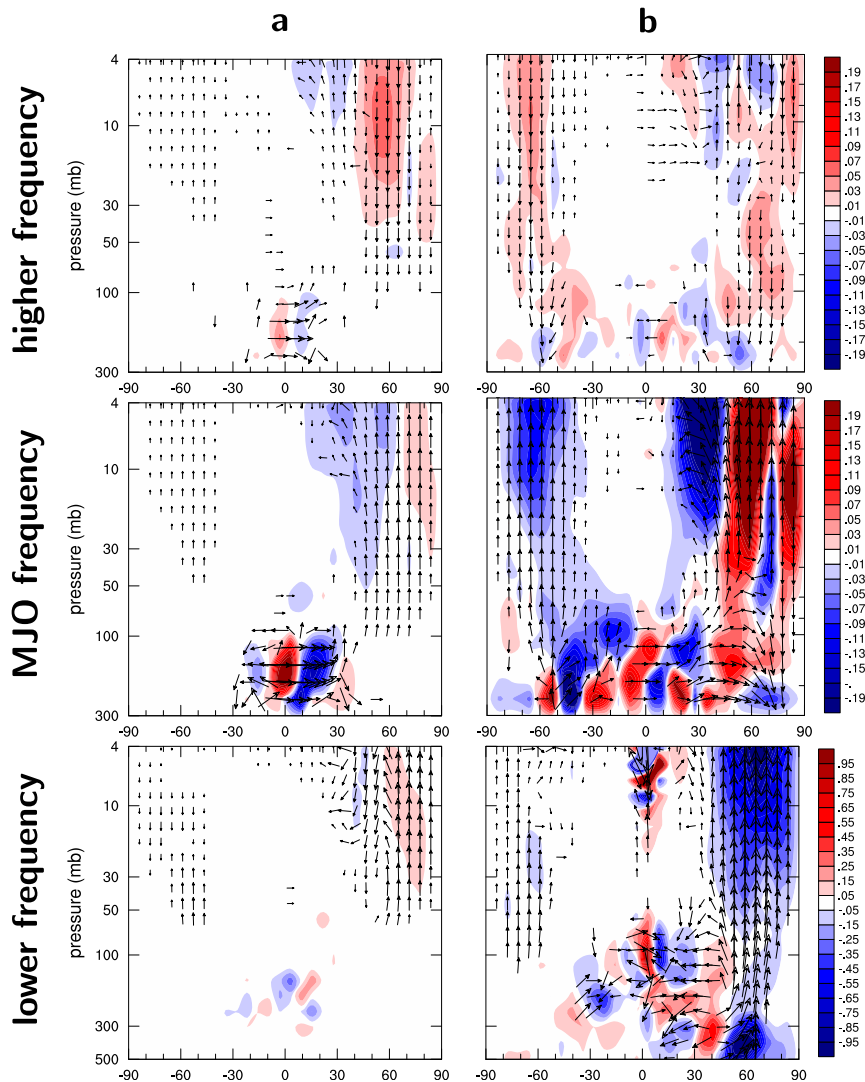


FIG. 5. EP flux changes in response to MJO forcing (forced minus unforced), at different frequency bands for (a) the idealized model and (b) WACCM. Arrows show EP flux change and shading shows EP flux divergence change ( $\text{m s}^{-1} \text{day}^{-1}$ ). The change is defined as the forced minus unforced results, filtered over the appropriate frequency band and averaged over time. The wind and temperature fields were first filtered to the corresponding frequency band and then used to evaluate the filtered EP flux. (top) EP flux contribution from frequency higher than the MJO frequency, (middle) MJO frequency (defined as 35–45 days for the idealized model and 20–100 days for WACCM), and (bottom) lower frequencies, including stationary waves. The EP flux is first scaled by pressure, and the length of the arrows is then adjusted to be proportional to the  $1/3$  power of the original EP flux to allow showing a larger range of EP flux. In (a), for the idealized model, the EP flux vectors and divergence below 100 mb are reduced by a factor of 10 to allow using the same color bar and vector scale as for the WACCM results in (b). Care must therefore be taken when comparing the arrows to the divergence shading around 100 mb and at high altitudes.

from  $30^\circ$  to  $70^\circ\text{N}$  by phases 6 and 7. Because it is difficult to identify the start point of this signal, the time scale for this horizontal propagation from the tropics to the high latitudes may only be roughly bounded between 10 and 20 days. This teleconnection time scale is roughly

consistent with the 10-day time scale found in previous works (Baldwin and Dunkerton 2001; Garfinkel et al. 2010; Seo and Son 2012; Lukens et al. 2017). An important caveat is that while the method we use to set the background of the idealized model is able to produce a

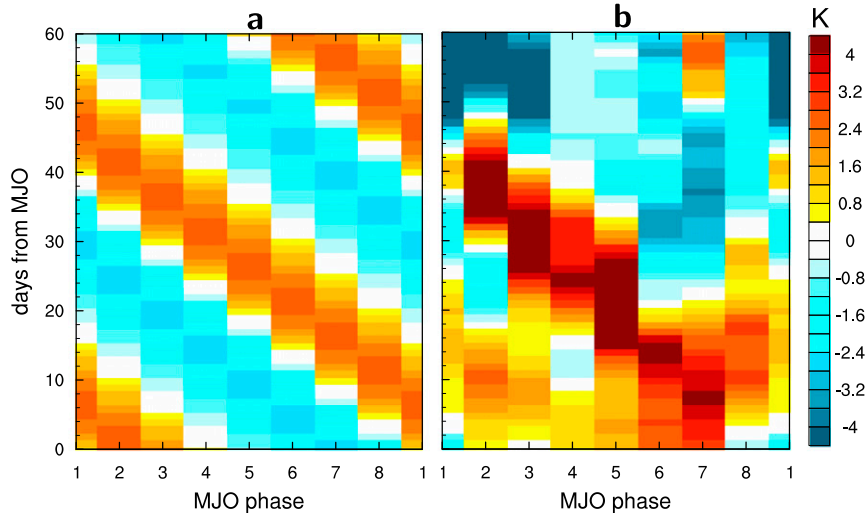


FIG. 6. Composite of polar cap ( $65^{\circ}$ – $90^{\circ}$ N and 10 mb) temperature (K), calculated as an average over all occurrences of a given MJO phase and shown as a function of that MJO phase (horizontal axis) and days since each phase (vertical axis), following Garfinkel et al. (2012a). Results are shown for (a) forced idealized model and (b) WACCM with enhanced entrainment and therefore stronger MJO.

reasonably realistic stratification and buoyancy frequency, some deviations from the actual stratification of the lower stratosphere could be affecting the propagation time scale of the MJO-forced waves in the idealized model. It is also possible that the Hovmöller diagrams in Fig. 7, used to represent the phase and group propagation,

are affected by a signal propagation that occurs at other pressure levels and affects the one shown. Note, for example, the discontinuity in the pseudomomentum diagram (Fig. 7c) at phase 6 and  $20^{\circ}$ N. Thus, we cannot exclude the possibility that the time scales deduced from these plots may be biased.

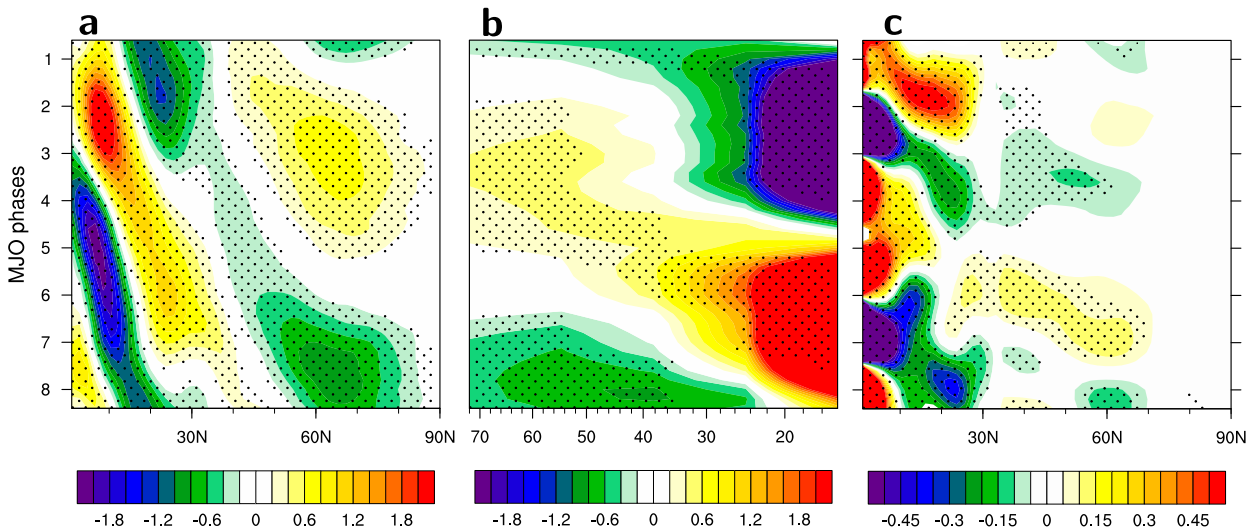


FIG. 7. Diagnostics of the meridional and vertical propagation of MJO-forced signal toward the Arctic stratosphere in the MJO-forced idealized model. Composites are calculated by averaging over all occurrences of a given MJO phase. (a) Latitude vs MJO phase composite of Ertel PV (PVU) at 60–80 mb showing the  $k = 1$  contribution averaged over  $90^{\circ}$ E– $180^{\circ}$ , reflecting horizontal phase propagation. (b) Pressure vs MJO phase composite of Ertel PV (PVU) averaged over  $70^{\circ}$ – $85^{\circ}$ N, again showing the contribution from  $k = 1$ , averaged over  $90^{\circ}$ E– $180^{\circ}$ , reflecting vertical phase propagation. (c) Latitude vs MJO phase composite of pseudomomentum flux ( $\text{m}^2 \text{s}^{-2}$ ) averaged over 60–80 mb, reflective of group propagation. Stippled areas are 95% statistically significant in (a) and (b) and 90% statistically significant in (c) using the Student's  $t$  test.

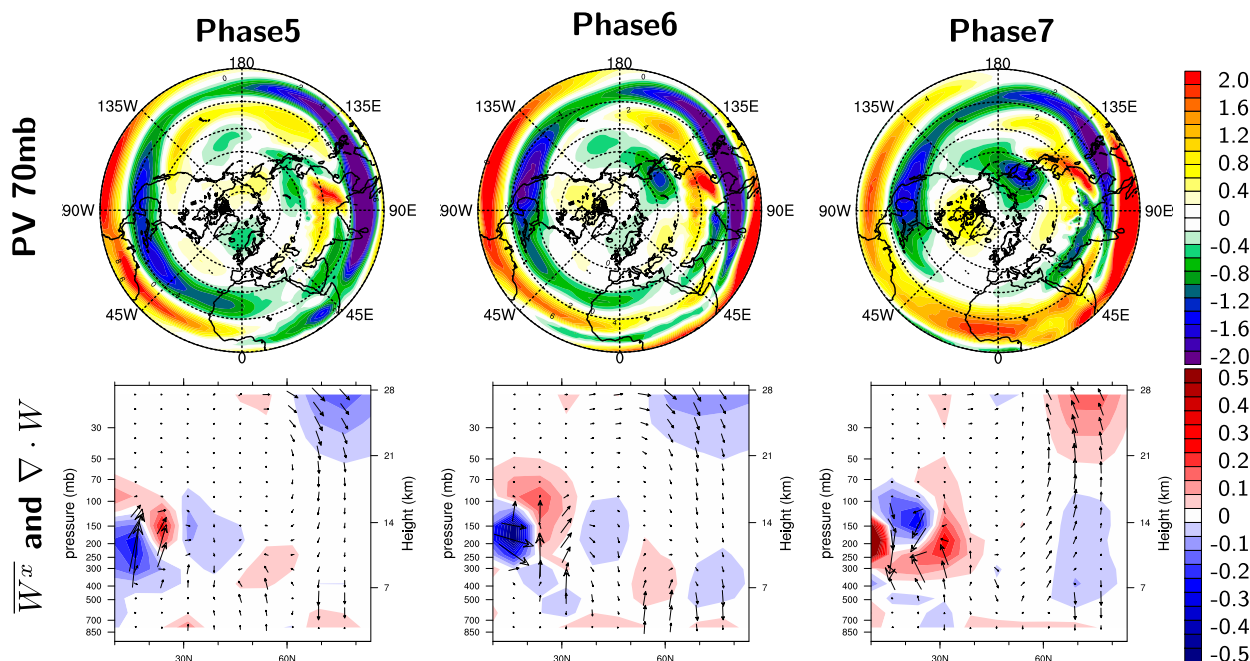


FIG. 8. Wave propagation diagnostics for the forced idealized model. (top) Ertel PV deviation (PVU) from the forced-run climatology, composited for (left)–(right) MJO phases 5, 6, and 7, averaged over 60–80 mb. (bottom) Zonally averaged wave pseudomomentum flux ( $\text{m}^2 \text{s}^{-2}$ ) deviation from the forced-run climatology due to  $k = 1$  waves (arrows) and its divergence ( $\text{m s}^{-1} \text{day}^{-1}$ ; color shading).

The spatial structure of the wave propagation in the idealized model is further analyzed in Fig. 8. Figure 8 (top) shows Ertel PV (in PVU;  $1 \text{ PVU} = 10^{-6} \text{ K kg}^{-1} \text{ m}^2 \text{ s}^{-1}$ ) anomalies from the forced-run climatology at 70 mb, showing a sequence of alternating sign perturbations propagating from the equator to the pole in the sector of  $90^\circ\text{E}$ – $180^\circ$  but also showing significant zonal phase propagation. The anomaly centers propagate slowly, consistent with the slow phase propagation mentioned before. Similar northward propagation also appears at other pressure levels between the upper troposphere and the lower stratosphere (not shown). We also ran additional idealized experiments (not shown) in which the idealized model was forced with a  $k = 1$ , 40-day period standing wave forcing. In one run, the maximum MJO forcing amplitude was prescribed at  $180^\circ$  (and  $0^\circ$ ) longitude and in another at  $90^\circ\text{E}$  (and  $90^\circ\text{W}$ ). The stratospheric response is seen when the forcing maximum is at  $180^\circ$  (and  $0^\circ$ ) longitude but not when it is at  $90^\circ\text{E}$  (and  $90^\circ\text{W}$ ). This again indicates that the wave source that leads to the stratospheric response is preferentially located slightly to the east of the longitudes that allow propagation.

Figure 8 (bottom) shows the contribution of  $k = 1$  planetary waves to the wave pseudomomentum flux and its divergence. They show that, in phases 5 and 6, a wave train propagating northward and upward between

$10^\circ$  and  $30^\circ\text{N}$  and then mostly poleward in the middle stratosphere, followed by downward propagation over the high latitudes. During phase 7 the northward propagation continues, with an upward propagation in the high latitudes. For later MJO phases, the pseudomomentum flux anomaly is downward (not shown), and the interpretation of the pseudomomentum fluxes is generally complicated by the existence of the positive feedback, which is inherent to the SSW mechanism (Matsuno 1971) and which leads to changes in the high-latitude vertical EP flux regardless of a possible triggering by MJO-forced waves. But the significant EP fluxes seen in the higher latitudes when compositing by the MJO phase clearly indicate a role for the MJO in triggering weak polar vortex events. We also calculated composites excluding SSW-associated days (not shown) and obtained identical results, indicating that the propagation does not depend on the SSW events and that MJO-forced waves can affect the Arctic stratosphere during non-SSW times. Note that the pseudomomentum flux anomalies shown in Figs. 7–10 are due to transient waves alone, since this flux includes only the product of two time anomalies [Eq. (A1)].

The propagation of the MJO-forced waves in WACCM is similarly analyzed in Figs. 9 and 10, where statistical significance is calculated as in Fig. 7. The pseudomomentum

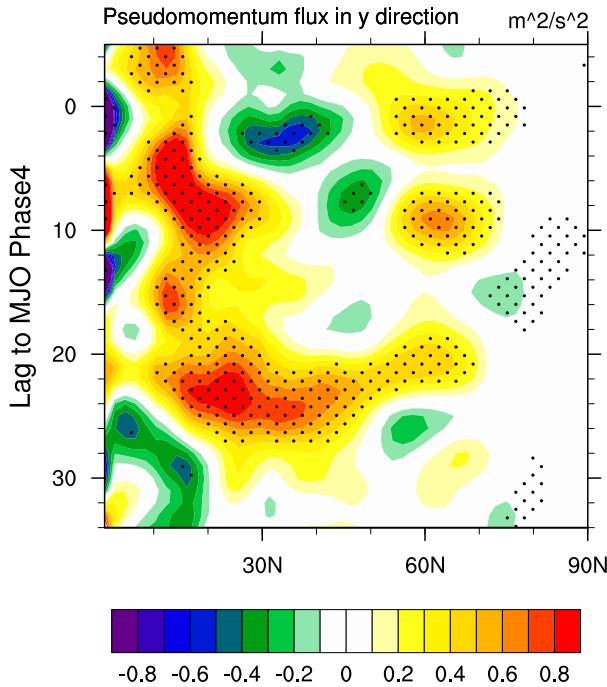


FIG. 9. Wave propagation diagnostics for WACCM, showing a composite of pseudomomentum meridional flux ( $\text{m}^2\text{s}^{-2}$ ) due to  $k = 1$  waves averaged between 180 and 120 mb, as a Hovmöller plot (lag relative to MJO phase 4 vs latitude). Stippled areas are 90% statistically significant according to the Student's  $t$  test.

flux composite shown in the Hovmöller plot of Fig. 9 again indicates a similar propagation time scale from the equator to near  $60^\circ\text{N}$ , although the signal is not as clear as in the idealized model. The horizontal phase propagation from the tropics to the polar cap similarly again indicates a strong zonal propagation (Fig. 10, top). Decomposing the PV anomalies by zonal wavenumbers (not shown) shows that the PV anomalies are dominated by  $k = 1$  in both models. The preferred longitudes of propagation in the two models seem to be influenced by the presence of the jet exit regions in the western Pacific and western Atlantic, which were shown to be important for quasi-stationary Rossby wave propagation (Simmons et al. 1983). We also note that Garfinkel et al. (2012a, 2014) similarly found the MJO to enhance the North Pacific climatological vertical stationary wave propagation. Figure 10 (bottom) shows the  $k = 1$  contribution to the wave pseudomomentum flux of Takaya and Nakamura (2001) and its divergence, composed by MJO phase. Similar comments as provided earlier for this idealized model apply here: there is clear propagation from the tropics, some in the upper troposphere and some (in composites based on additional MJO phases; not

shown) in the lower stratosphere. Again the flux cannot be attributed only to the MJO forcing as a result of the positive feedback involved in the SSW mechanism, but the significant fluxes clearly demonstrate an MJO role in SSW dynamics and, in particular, leading to the increased SSW frequency in WACCM.

The horizontal path of wave propagation is not identical in the two models used here, and this may be related to the difference in climatology and MJO forcing in the two models. The zonal symmetry is broken by two factors: first, the longitude range in which the MJO is active, from the Indian Ocean to the middle of the Pacific Ocean (Zhang 2005), and second, the longitude range in which the subtropical tropospheric jet is weakening going eastward (e.g., Bao and Hartmann 2014). The interplay of these two factors, along with the difference between the location of the jet and MJO source characteristics, sets the longitude range of propagation, and relatively small differences in these two factors between the two models lead to different propagation longitude ranges.

Overall, the above diagnostics show a direct propagation of MJO-forced transient waves from the tropics to the Arctic stratosphere, where they play a role in MJO–SSW teleconnection. We next discuss the stationary wave response.

### c. Teleconnection mechanism: Stationary wave response

In addition to the direct propagation of transient waves from the MJO to the Arctic stratosphere proposed and diagnosed above, the temperature budget shown in Fig. 4 indicates that the stationary wave heat flux increases in the MJO-forced cases, which requires a nonlinear interaction between the transient MJO-forced waves and the background flow. We note again that the stationary wave response is different from the constructive interference of Garfinkel et al. (2014), which vanishes in a time-averaged budget analysis. The purpose of this section is to investigate this strengthening of the stationary waves.

We start by decomposing the stationary heat transport change resulting from MJO forcing [lhs of Eq. (2)] into the contribution from temperature response alone [the first term on rhs of Eq. (2)], the contribution from meridional wind response alone (second term), and the contribution from the correlation between the two responses (last term):

$$\begin{aligned} & \langle \bar{V}_{\text{MJO}}^* \bar{T}_{\text{MJO}}^* \rangle - \langle \bar{V}_{\text{CTRL}}^* \bar{T}_{\text{CTRL}}^* \rangle \\ &= \langle \bar{V}_{\text{CTRL}}^* \Delta \bar{T}^* \rangle + \langle \bar{T}_{\text{CTRL}}^* \Delta \bar{V}^* \rangle + \langle \Delta \bar{V}^* \Delta \bar{T}^* \rangle. \end{aligned} \quad (2)$$

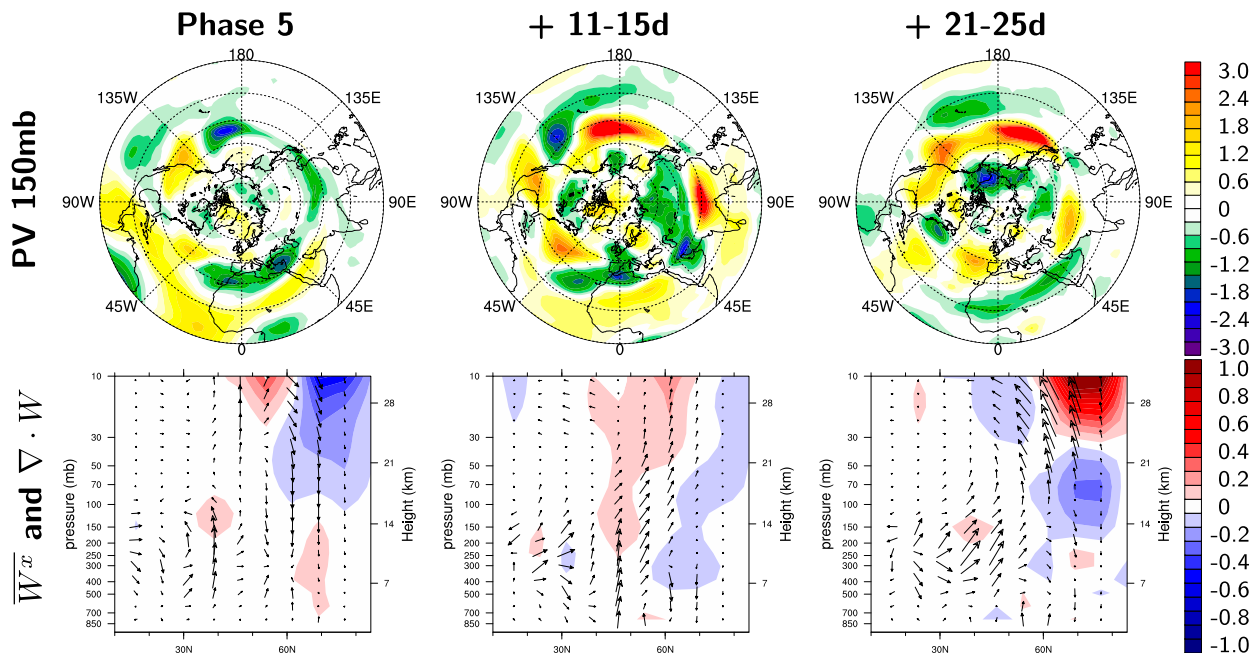


FIG. 10. As in Fig. 8, but for wave propagation diagnostics for WACCM except that the composites account for DJF only, and (left) MJO phase 5 and two periods of (center) 11–15 and (right) 21–25 days relative to phase 5 are shown.

Figure 11 shows the three terms in Eq. (2) as a function of pressure and latitude. The term due to change in the temperature only (Fig. 11, left) is clearly the dominant contribution to the heat transport.

Next, to diagnose the contributions to the stationary wave heat flux by different zonal wavenumbers, Fig. 12 shows the decomposition of the stationary wave heat transport  $\langle \bar{V}^* \bar{T}^* \rangle$  and the stationary temperature variance  $\langle (\bar{T}^*)^2 \rangle$  into wavenumbers 1, 2, and 3, for both the forced and unforced runs and for both the idealized model and WACCM, averaged over 80–120 mb. The stationary wave temperature variance enhancement due to the MJO forcing (Fig. 12, top; compare red to black lines) is maximal at 60°N in the idealized model and at

65°N in WACCM. The contribution of wavenumber  $k = 1$  dominates in both the idealized model and WACCM, and  $k = 2$  also plays a nonnegligible role in WACCM. As expected, we also found that the variance of  $\bar{V}^*$  does not increase significantly (not shown) and that the correlation between  $\bar{T}^*$  and  $\bar{V}^*$  does not increase significantly (not shown), which verifies that the increase in the variance of  $\bar{T}^*$  is the main mechanism behind the increase in the heat flux.

The final step is to understand which processes lead to the dominance of the term  $\langle \bar{V}_{\text{CTRL}}^* \Delta \bar{T}^* \rangle$ . To diagnose this, we multiply the time-averaged terms of the temperature equation by  $\bar{V}_{\text{CTRL}}^*$  to find an equation of the form  $\bar{V}_{\text{CTRL}}^* \partial T / \partial t = \dots$  and then zonally average to find

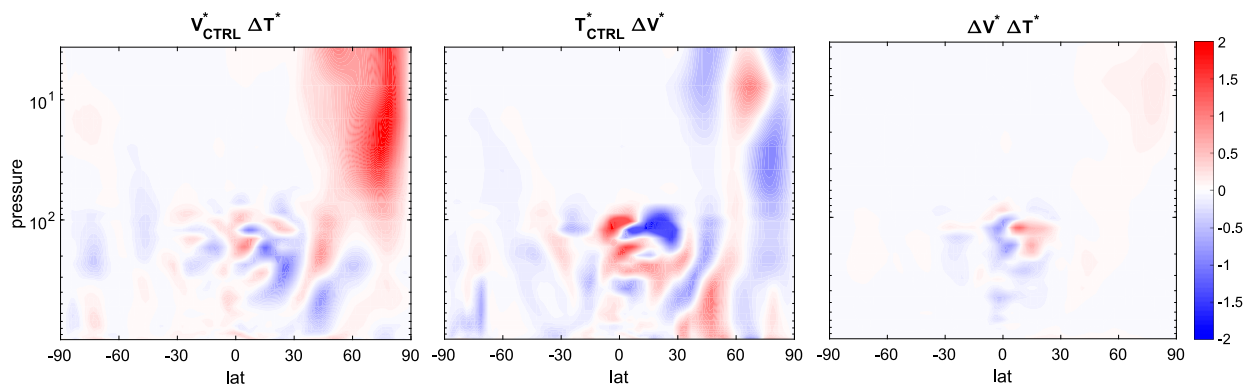


FIG. 11. Idealized model stationary eddy heat transport ( $\text{m s}^{-1} \text{K}$ ) due to (left) change in the climatological  $T$  alone, (center) change in the climatological  $V$  alone, and (right) the cross term of change in  $T$  and  $V$ . See text for details.

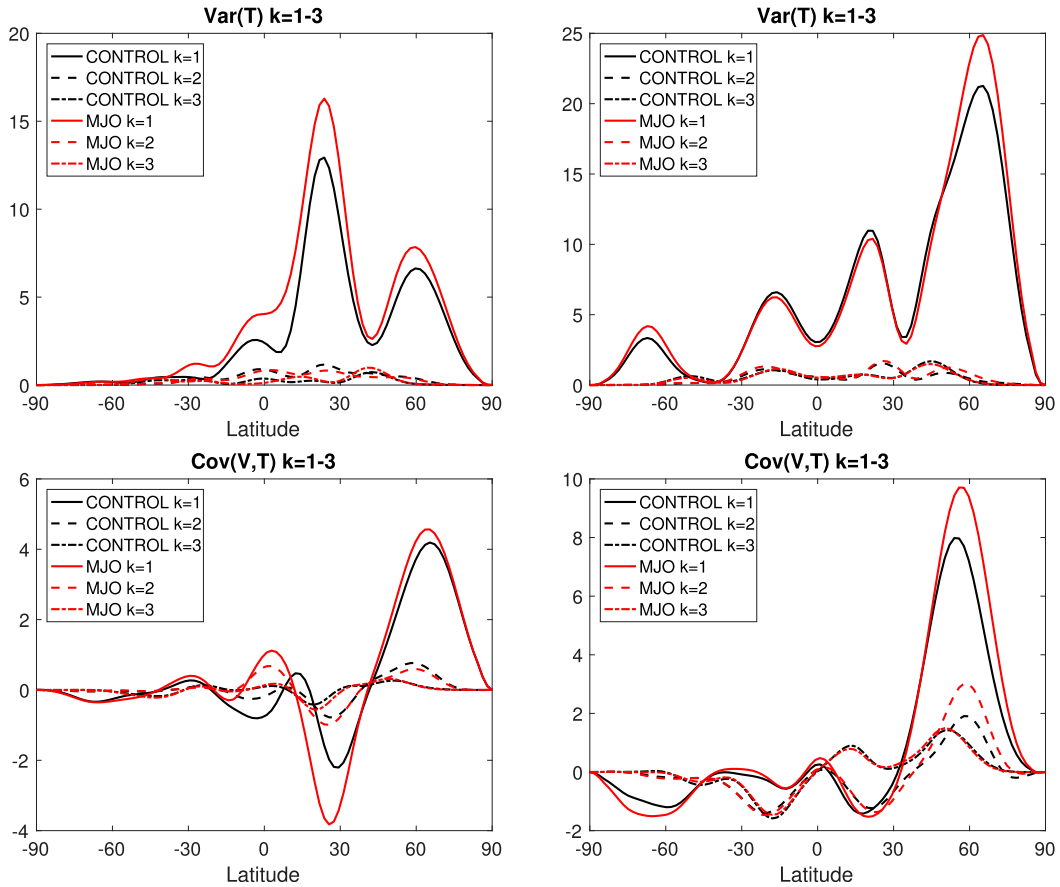


FIG. 12. Contribution of zonal wavenumbers 1–3 to the stationary wave meridional heat flux in (left) the idealized model and (right) WACCM, averaged over 80–120 mb. (top) Variance of temperature signal ( $\text{K}^2$ ) due to stationary waves  $\bar{T}^*$ . (bottom) The stationary wave heat flux ( $\overline{V^* \bar{T}^*}$ ) at 100 mb ( $\text{m s}^{-1} \text{K}$ ). Contribution is shown for  $k = 1$  (thin solid line),  $k = 2$  (thin dashed line),  $k = 3$  (thin dot-dashed line). Red lines show MJO-forced experiments, and black lines show the unforced control experiments.

the projection of each term on the stationary wave component  $\bar{V}_{\text{CTRL}}^*$ . This allows us to find which terms in the temperature equation contribute to the increase in  $\langle \bar{V}_{\text{CTRL}}^* \bar{T}^* \rangle$  as a result of MJO forcing. We find that both the mean meridional heat transport and the eddy meridional heat transport are positive and significant when projected on  $\bar{V}_{\text{CTRL}}^*$ . Finally, we find that the contributions of vertical advection terms to  $\langle \bar{V}_{\text{CTRL}}^* \bar{T}^* \rangle$  are negligible, while zonal heat transport terms contribute negatively, to balance that of the meridional terms, as the net change must vanish.

#### 4. Conclusions

The goal of this work was to examine the response of the polar stratospheric vortex, and sudden stratospheric warming (SSW) events in particular, to a strengthening of the Madden–Julian oscillation (MJO) expected in a warmer climate (e.g., Arnold et al. 2014). We were also

interested in some aspects of the teleconnection mechanism between the MJO and SSW that are not completely understood. To explore these issues, we analyzed an idealized dry atmospheric model with and without an added idealized MJO forcing. We also analyzed a more realistic GCM (WACCM), with and without a strengthened MJO amplitude obtained by increasing the convective entrainment rate.

With a stronger MJO forcing, we find that both the idealized model and WACCM show a significant increase of the SSW frequency and a warmer Arctic stratosphere averaged climatology. This is consistent with and explains the warmer Arctic stratospheric climatology noted by Arnold et al. (2014) in a  $4 \times \text{CO}_2$  simulation, confirming that the response in this superparameterized model may indeed be due to the strengthening of the MJO seen in that study. The quantitative increase in SSW frequency is robust, and the magnitude of the increase in a warmer future climate

would depend, of course, on the amplitude of the increase in MJO (sections 2b and 2c). The similar response in the two models suggests that dry processes dominate the teleconnection mechanism.

Previous studies did not clearly address the pathway whereby the MJO affects SSW, and specifically, Garfinkel et al. (2014) showed changes to high-latitude wave heat flux resulting from MJO forcing, but the path of propagation was not analyzed explicitly. We find that both MJO-forced transient waves and stationary waves play a role in the teleconnection. Composite analysis of the idealized model PV field clearly shows a transient wave train initiating from the MJO region, propagating through the upper troposphere and the lower stratosphere and then propagating farther upward at high latitudes. In addition to the direct propagation of transient MJO-forced waves into the Arctic stratosphere, we find that in both models considered here, the MJO-forced waves enhance the  $k = 1$  stationary wave heat flux reaching the stratosphere. The MJO-forced waves increase the stationary temperature variance at high latitudes in the upper troposphere and stratosphere, and this leads to an enhanced stationary wave heat flux in the Arctic stratosphere that contributes to the heat budget there and therefore likely to the changes in SSW frequency. The mechanism leading to the increase in the high-latitude stationary temperature variance involves both mean and eddy meridional heat transports that enhance the stationary zonally asymmetric temperature signal, which projects on the corresponding zonally asymmetric meridional mean velocity signal.

The teleconnection time scale is another factor considered here. Garfinkel et al. (2012a, 2014) find that MJO phase 7 occurs 1–12 days before SSW events, and MJO phase 4 occurs 13–24 days before SSW events. While this seems to suggest a 3-week teleconnection time scale, they also find correlation between the MJO and the polar cap at lags exceeding 40 days. Our idealized model, with its perfectly periodic prescribed MJO forcing, allows us to identify the propagating signal in a Hovmöller plot of pseudomomentum flux with some confidence. While this analysis cannot determine the teleconnection time scale with certainty, it suggests a horizontal propagation time scale between 10 and 20 days, and we point out uncertainties in this estimate. This horizontal propagation is followed by additional time for vertical propagation within the stratosphere.

Our idealized model, while helpful in obtaining clean results for the teleconnection time scale and mechanism, is highly simplified, and the results are therefore to be viewed with care. Similarly, the method we used to increase the MJO amplitude in the more realistic WACCM via an increase in the entrainment rate is

known to produce mean state biases that could influence the MJO–SSW teleconnection. What is needed is to verify these results in a model such as the superparameterized model that produces a realistic MJO simulation (Grabowski 2001; Randall et al. 2003) that explicitly simulates the increase in MJO amplitude (Arnold et al. 2013, 2014, 2015), which at the same time also resolves the stratospheric dynamics. We have also considered all SSW events as a single category, while it is known that displacement and split SSW events have different life cycles and different precursors (Andrews et al. 1987; Charlton and Polvani 2007), and the effect of the MJO on these events could therefore be different as well.

Given that the MJO is predicted to be stronger in a warmer future climate (see references in introduction section), the increased SSW frequency resulting from the strengthened MJO found here also suggests a warmer winter Arctic stratosphere climatology, as indicated by the preliminary results of Arnold et al. (2014). This mechanism may have therefore contributed to the observed winter warming trend in the Arctic lower stratosphere during past decades (Bohlinger et al. 2014). An increased SSW frequency would also lead to the known downward propagation teleconnections, affecting the Arctic Oscillation, midlatitude blocking systems, and extreme weather events (e.g., Baldwin and Dunkerton 1999; Gerber and Polvani 2009; Thompson et al. 2002; Cohen et al. 2007; Kolstad et al. 2010). However, other changes due to global warming, such as changes in the meridional temperature gradient, in the strength of the tropospheric jets, or in stratospheric temperature and circulation, may affect wave propagation and change the way that MJO activity affects the Arctic stratosphere. In addition, downward propagation of SSW events, along with their effect on extreme weather, may be different in a warmer climate. This study isolated the effect of the MJO amplitude on SSW frequency in order to understand the relevant mechanisms, but these caveats suggest care in applying the conclusions to an actual warming scenario. With these caveats in mind, we note that the long time scale of the MJO–SSW teleconnection suggests a long predictability time scale and, together with the expected MJO strengthening in a warmer climate, suggests that further study of this teleconnection is needed.

*Acknowledgments.* This work was funded by the NSF P2C2 program Grant OCE-1602864 and by the Harvard Global Institute and Harvard Climate Solutions funds. ET thanks the Weizmann Institute for its hospitality during parts of this work. We would like to acknowledge high-performance computing support from Yellowstone provided by NCAR's Computational and Information

Systems Laboratory, sponsored by the National Science Foundation.

## APPENDIX

### Calculation of the Instantaneous 3D Wave Activity Flux

The instant wave activity flux used here extends the EP flux to three dimensions and was defined and

shown to be a useful diagnostic for wave activity by Takaya and Nakamura (2001). Equation (A1) shows the wave activity flux in the longitudinal, latitudinal, and vertical directions, in spherical coordinates. In this equation,  $\psi'$  denotes the geostrophic streamfunction anomaly in pressure coordinates,  $U$  and  $V$  denote 30-day time-averaged zonal and meridional winds, primes denote deviations from these averages,  $p$  is pressure,  $S$  is the static stability,  $R$  is the gas constant, and  $a$  is Earth's radius:

$$\begin{aligned} W_\phi &= \frac{p \cos\phi}{2|U|} \left[ U \left( v'^2 - \psi' \frac{1}{a \cos\phi} \frac{\partial v'}{\partial \lambda} \right) - V \left( -u'v' + \psi' \frac{1}{a \cos\phi} \frac{\partial u'}{\partial \lambda} \right) \right], \\ W_\theta &= \frac{p \cos\phi}{2|U|} \left[ U \left( -u'v' + \psi' \frac{1}{a \cos\phi} \frac{\partial u'}{\partial \lambda} \right) + V \left( u'^2 + \psi' \frac{1}{a} \frac{\partial u'}{\partial \phi} \right) \right], \text{ and} \\ W_z &= \frac{\cos\phi}{2|U|} \frac{fR}{S^2g} \left[ U \left( v'T' - \psi' \frac{1}{a \cos\phi} \frac{\partial T'}{\partial \lambda} \right) - V \left( -u'T' - \psi' \frac{1}{a} \frac{\partial T'}{\partial \phi} \right) \right]. \end{aligned} \quad (\text{A1})$$

## REFERENCES

- Andrews, D. G., J. R. Holton, and C. B. Leovy, 1987: *Middle Atmosphere Dynamics*. Academic Press, 489 pp.
- Arnold, N., Z. Kuang, and E. Tziperman, 2013: Enhanced MJO-like variability at high SST. *J. Climate*, **26**, 988–1001, doi:10.1175/JCLI-D-12-00272.1.
- , M. Branson, M. A. Burt, D. S. Abbot, Z. Kuang, D. A. Randall, and E. Tziperman, 2014: Effects of explicit atmospheric convection at high CO<sub>2</sub>. *Proc. Natl. Acad. Sci. USA*, **111**, 10 943–10 948, doi:10.1073/pnas.1407175111.
- , —, Z. Kuang, D. A. Randall, and E. Tziperman, 2015: MJO intensification with warming in the superparameterized CESM. *J. Climate*, **28**, 2706–2724, doi:10.1175/JCLI-D-14-00494.1.
- Baldwin, M., and T. Dunkerton, 1999: Propagation of the Arctic Oscillation from the stratosphere to the troposphere. *J. Geophys. Res.*, **104**, 30 937–30 946, doi:10.1029/1999JD900445.
- , and —, 2001: Stratospheric harbingers of anomalous weather regimes. *Science*, **294**, 581–584, doi:10.1126/science.1063315.
- Bao, M., and D. L. Hartmann, 2014: The response to MJO-like forcing in a nonlinear shallow-water model. *Geophys. Res. Lett.*, **41**, 1322–1328, doi:10.1002/2013GL057683.
- Bell, C. J., L. J. Gray, and J. Kettleborough, 2010: Changes in Northern Hemisphere stratospheric variability under increased CO<sub>2</sub> concentrations. *Quart. J. Roy. Meteor. Soc.*, **136**, 1181–1190, doi:10.1002/qj.633.
- Benedict, J. J., E. D. Maloney, A. H. Sobel, D. M. Frierson, and L. J. Donner, 2013: Tropical intraseasonal variability in version 3 of the GFDL atmosphere model. *J. Climate*, **26**, 426–449, doi:10.1175/JCLI-D-12-00103.1.
- Bohlinger, P., B. M. Sinnhuber, R. Ruhnke, and O. Kirner, 2014: Radiative and dynamical contributions to past and future Arctic stratospheric temperature trends. *Atmos. Chem. Phys.*, **14**, 1679–1688, doi:10.5194/acp-14-1679-2014.
- Butchart, N., J. Austin, J. R. Knight, A. A. Scaife, and M. L. Gallani, 2000: The response of the stratospheric climate to projected changes in the concentrations of well-mixed greenhouse gases from 1992 to 2051. *J. Climate*, **13**, 2142–2159, doi:10.1175/1520-0442(2000)013<2142:TROTSC>2.0.CO;2.
- Butler, A. H., D. J. Seidel, S. C. Hardiman, N. Butchart, T. Birner, and A. Match, 2015: Defining sudden stratospheric warmings. *Bull. Amer. Meteor. Soc.*, **96**, 1913–1928, doi:10.1175/BAMS-D-13-00173.1.
- Caballero, R., and M. Huber, 2010: Spontaneous transition to superrotation in warm climates simulated by CAM3. *Geophys. Res. Lett.*, **37**, L11701, doi:10.1029/2010GL043468.
- Cassou, C., 2008: Intraseasonal interaction between the Madden-Julian oscillation and the North Atlantic Oscillation. *Nature*, **455**, 523–527, doi:10.1038/nature07286.
- Charlton, A. J., and L. M. Polvani, 2007: A new look at stratospheric sudden warmings. Part I: Climatology and modeling benchmarks. *J. Climate*, **20**, 449–469, doi:10.1175/JCLI3996.1.
- Charlton-Perez, A. J., L. M. Polvani, J. Austin, and F. Li, 2008: The frequency and dynamics of stratospheric sudden warmings in the 21st century. *J. Geophys. Res.*, **113**, D16116, doi:10.1029/2007JD009571.
- Cohen, J., M. Barlow, P. Kushner, and K. Saito, 2007: Stratosphere–troposphere coupling and links with Eurasian land surface variability. *J. Climate*, **20**, 5335–5343, doi:10.1175/2007JCLI1725.1.
- Craig, R. A., W. S. Hering, R. A. Craig, and W. S. Hering, 1959: The stratospheric warming of January–February 1957. *J. Meteor.*, **16**, 91–107, doi:10.1175/1520-0469(1959)016<0091:TSWOJF>2.0.CO;2.
- Garfinkel, C. I., and D. L. Hartmann, 2008: Different ENSO teleconnections and their effects on the stratospheric polar vortex. *J. Geophys. Res.*, **113**, D18114, doi:10.1029/2008JD009920.
- , —, and F. Sassi, 2010: Tropospheric precursors of anomalous Northern Hemisphere stratospheric polar vortices. *J. Climate*, **23**, 3282–3299, doi:10.1175/2010JCLI3010.1.
- , S. B. Feldstein, D. W. Waugh, C. Yoo, and S. Lee, 2012a: Observed connection between stratospheric sudden warmings and the Madden-Julian Oscillation. *Geophys. Res. Lett.*, **39**, L18807, doi:10.1029/2012GL053144.
- , T. A. Shaw, D. L. Hartmann, and D. W. Waugh, 2012b: Does the Holton–Tan mechanism explain how the quasi-biennial oscillation modulates the Arctic polar vortex? *J. Atmos. Sci.*, **69**, 1713–1733, doi:10.1175/JAS-D-11-0209.1.

- , J. J. Benedict, and E. D. Maloney, 2014: Impact of the MJO on the boreal winter extratropical circulation. *Geophys. Res. Lett.*, **41**, 6055–6062, doi:10.1002/2014GL061094.
- Gerber, E. P., and L. M. Polvani, 2009: Stratosphere–troposphere coupling in a relatively simple AGCM: The importance of stratospheric variability. *J. Climate*, **22**, 1920–1933, doi:10.1175/2008JCLI2548.1.
- Goss, M., S. B. Feldstein, and S. Lee, 2016: Stationary wave interference and its relation to tropical convection and Arctic warming. *J. Climate*, **29**, 1369–1389, doi:10.1175/JCLI-D-15-0267.1.
- Grabowski, W. W., 2001: Coupling cloud processes with the large-scale dynamics using the cloud-resolving convection parameterization (CRCP). *J. Atmos. Sci.*, **58**, 978–997, doi:10.1175/1520-0469(2001)058<0978:CCPWTL>2.0.CO;2.
- Hall, N., 2000: A simple GCM based on dry dynamics and constant forcing. *J. Atmos. Sci.*, **57**, 1557–1572, doi:10.1175/1520-0469(2000)057<1557:ASGBOD>2.0.CO;2.
- Hardiman, S. C., P. J. Kushner, and J. Cohen, 2008: Investigating the ability of general circulation models to capture the effects of Eurasian snow cover on winter climate. *J. Geophys. Res.*, **113**, D21123, doi:10.1029/2008JD010623.
- Harnik, N., and R. S. Lindzen, 2001: The effect of reflecting surfaces on the vertical structure and variability of stratospheric planetary waves. *J. Atmos. Sci.*, **58**, 2872–2894, doi:10.1175/1520-0469(2001)058<2872:TEORSO>2.0.CO;2.
- Held, I. M., and M. J. Suarez, 1994: A proposal for the intercomparison of the dynamical cores of atmospheric general circulation models. *Bull. Amer. Meteor. Soc.*, **75**, 1825–1830, doi:10.1175/1520-0477(1994)075<1825:APFTIO>2.0.CO;2.
- Hendon, H. H., C. Zhang, and J. D. Glick, 1999: Interannual variation of the Madden–Julian oscillation during austral summer. *J. Climate*, **12**, 2538–2550, doi:10.1175/1520-0442(1999)012<2538:IVOTMJ>2.0.CO;2.
- Holton, J. R., and H.-C. Tan, 1980: The influence of the equatorial quasi-biennial oscillation on the global circulation at 50 mb. *J. Atmos. Sci.*, **37**, 2200–2208, doi:10.1175/1520-0469(1980)037<2200:TIOTEQ>2.0.CO;2.
- Hurwitz, M. M., P. A. Newman, and C. I. Garfinkel, 2012: On the influence of North Pacific sea surface temperature on the Arctic winter climate. *J. Geophys. Res.*, **117**, D19110, doi:10.1029/2012JD017819.
- Inness, P. M., J. M. Slingo, P. M. Inness, and J. M. Slingo, 2003: Simulation of the Madden–Julian oscillation in a coupled general circulation model. Part I: Comparison with observations and an atmosphere-only GCM. *J. Climate*, **16**, 345–364, doi:10.1175/1520-0442(2003)016<0345:SOTMJO>2.0.CO;2.
- Jones, C., and L. M. V. Carvalho, 2006: Changes in the activity of the Madden–Julian Oscillation during 1958–2004. *J. Climate*, **19**, 6353–6370, doi:10.1175/JCLI3972.1.
- Karoly, D., and B. Hoskins, 1982: Three dimensional propagation of planetary waves. *J. Meteor. Soc. Japan*, **60**, 109–122, doi:10.2151/jmsj1965.60.1\_109.
- Klein, S. A., J. S. Boyle, J. Tannahill, D. Lucas, R. B. Neale, S. Xie, and K. R. Sperber, 2012: Perturbed-parameter hindcasts of the MJO with CAM5. *2012 Fall Meeting*, San Francisco, CA, Amer. Geophys. Union, Abstract A52D-06.
- Kolstad, E. W., T. Breiteig, and A. A. Scaife, 2010: The association between stratospheric weak polar vortex events and cold air outbreaks in the Northern Hemisphere. *Quart. J. Roy. Meteor. Soc.*, **136**, 886–893, doi:10.1002/qj.620.
- Kushner, P. J., and L. M. Polvani, 2004: Stratosphere–troposphere coupling in a relatively simple AGCM: The role of eddies. *J. Climate*, **17**, 629–639, doi:10.1175/1520-0442(2004)017<0629:SCIARS>2.0.CO;2.
- Lee, S., 1999: Why are the climatological zonal winds easterly in the equatorial upper troposphere? *J. Atmos. Sci.*, **56**, 1353–1363, doi:10.1175/1520-0469(1999)056<1353:WATCZW>2.0.CO;2.
- Limpasuvan, V., D. Thompson, and D. Hartmann, 2004: The life cycle of the Northern Hemisphere sudden stratospheric warmings. *J. Climate*, **17**, 2584–2596, doi:10.1175/1520-0442(2004)017<2584:TLCOTN>2.0.CO;2.
- Liu, C., B. Tian, K.-F. Li, G. L. Manney, N. J. Livesey, Y. L. Yung, and D. E. Waliser, 2014: Northern Hemisphere mid-winter vortex-displacement and vortex-split stratospheric sudden warmings: Influence of the Madden-Julian oscillation and quasi-biennial oscillation. *J. Geophys. Res. Atmos.*, **119**, 12 599–12 620, doi:10.1002/2014JD021876.
- Lukens, K. E., S. B. Feldstein, C. Yoo, and S. Lee, 2017: The dynamics of the extratropical response to Madden–Julian oscillation convection. *Quart. J. Roy. Meteor. Soc.*, **143**, 1095–1106, doi:10.1002/qj.2993.
- Madden, R. A., and P. R. Julian, 1971: Detection of a 40–50 day oscillation in zonal wind in tropical Pacific. *J. Atmos. Sci.*, **28**, 702–708, doi:10.1175/1520-0469(1971)028<0702:DOADOI>2.0.CO;2.
- Marsh, D. R., M. J. Mills, D. E. Kinnison, J.-F. Lamarque, N. Calvo, and L. M. Polvani, 2013: Climate change from 1850 to 2005 simulated in CESM1 (WACCM). *J. Climate*, **26**, 7372–7391, doi:10.1175/JCLI-D-12-00558.1.
- Matsuno, T., 1971: A dynamical model of the stratospheric sudden warming. *J. Atmos. Sci.*, **28**, 1479–1494, doi:10.1175/1520-0469(1971)028<1479:ADMOTS>2.0.CO;2.
- McLandress, C., and T. G. Shepherd, 2009: Impact of climate change on stratospheric sudden warmings as simulated by the Canadian Middle Atmosphere Model. *J. Climate*, **22**, 5449–5463, doi:10.1175/2009JCLI3069.1.
- Mitchell, D. M., S. M. Osprey, L. J. Gray, N. Butchart, S. C. Hardiman, A. J. Charlton-Perez, and P. Watson, 2012: The effect of climate change on the variability of the Northern Hemisphere stratospheric polar vortex. *J. Atmos. Sci.*, **69**, 2608–2618, doi:10.1175/JAS-D-12-021.1.
- Neale, R. B., and Coauthors, 2010: Description of the NCAR Community Atmosphere Model (CAM 4.0). NCAR Tech. Note NCAR/TN-485+STR, 224 pp., [http://www.cesm.ucar.edu/models/ccsm4.0/cam/docs/description/cam4\\_desc.pdf](http://www.cesm.ucar.edu/models/ccsm4.0/cam/docs/description/cam4_desc.pdf).
- Oliver, E. C., and K. R. Thompson, 2012: A reconstruction of Madden–Julian oscillation variability from 1905 to 2008. *J. Climate*, **25**, 1996–2019, doi:10.1175/JCLI-D-11-00154.1.
- Randall, D., M. Khairoutdinov, A. Arakawa, and W. Grabowski, 2003: Breaking the cloud parameterization deadlock. *Bull. Amer. Meteor. Soc.*, **84**, 1547–1564, doi:10.1175/BAMS-84-11-1547.
- Richter, J. H., A. Solomon, and J. T. Bacmeister, 2014: Effects of vertical resolution and nonorographic gravity wave drag on the simulated climate in the Community Atmosphere Model, version 5. *J. Adv. Model. Earth Syst.*, **6**, 357–383, doi:10.1002/2013MS000303.
- Schimanke, S., T. Spanghel, H. Huebener, and U. Cubasch, 2013: Variability and trends of major stratospheric warmings in simulations under constant and increasing GHG concentrations. *Climate Dyn.*, **40**, 1733–1747, doi:10.1007/s00382-012-1530-x.
- Schubert, J. J., B. Stevens, and T. Crueger, 2013: Madden-Julian oscillation as simulated by the MPI Earth system model: Over the last and into the next millennium. *J. Adv. Model. Earth Syst.*, **5**, 71–84, doi:10.1029/2012MS000180.

- Seo, K.-H., and S.-W. Son, 2012: The global atmospheric circulation response to tropical diabatic heating associated with the Madden–Julian oscillation during northern winter. *J. Atmos. Sci.*, **69**, 79–96, doi:[10.1175/2011JAS3686.1](https://doi.org/10.1175/2011JAS3686.1).
- Simmons, A. J., J. M. Wallace, and G. W. Branstator, 1983: Barotropic wave propagation and instability, and atmospheric teleconnection patterns. *J. Atmos. Sci.*, **40**, 1363–1392, doi:[10.1175/1520-0469\(1983\)040<1363:BWPAlA>2.0.CO;2](https://doi.org/10.1175/1520-0469(1983)040<1363:BWPAlA>2.0.CO;2).
- Slingo, J., D. Rowell, K. Sperber, and E. Nortley, 1999: On the predictability of the interannual behaviour of the Madden–Julian oscillation and its relationship with El Niño. *Quart. J. Roy. Meteor. Soc.*, **125**, 583–609, doi:[10.1002/qj.49712555411](https://doi.org/10.1002/qj.49712555411).
- Smith, K. L., R. R. Neely, D. R. Marsh, and L. M. Polvani, 2014: The Specified Chemistry Whole Atmosphere Community Climate Model (SC-WACCM). *J. Adv. Model. Earth Syst.*, **6**, 883–901, doi:[10.1002/2014MS000346](https://doi.org/10.1002/2014MS000346).
- Subramanian, A. C., M. Jochum, A. Miller, R. Murtugudde, R. Neale, and D. Waliser, 2011: The Madden–Julian oscillation in CCSM4. *J. Climate*, **24**, 6261–6282, doi:[10.1175/JCLI-D-11-00031.1](https://doi.org/10.1175/JCLI-D-11-00031.1).
- Takaya, K., and H. Nakamura, 2001: A formulation of a phase-independent wave-activity flux for stationary and migratory quasigeostrophic eddies on a zonally varying basic flow. *J. Atmos. Sci.*, **58**, 608–627, doi:[10.1175/1520-0469\(2001\)058<0608:AFOAPI>2.0.CO;2](https://doi.org/10.1175/1520-0469(2001)058<0608:AFOAPI>2.0.CO;2).
- Thompson, D. W. J., M. P. Baldwin, and J. M. Wallace, 2002: Stratospheric connection to Northern Hemisphere wintertime weather: Implications for prediction. *J. Climate*, **15**, 1421–1428, doi:[10.1175/1520-0442\(2002\)015<1421:SCTNHW>2.0.CO;2](https://doi.org/10.1175/1520-0442(2002)015<1421:SCTNHW>2.0.CO;2).
- Wheeler, M., and G. N. Kiladis, 1999: Convectively coupled equatorial waves: Analysis of clouds and temperature in the wavenumber–frequency domain. *J. Atmos. Sci.*, **56**, 374–399, doi:[10.1175/1520-0469\(1999\)056<0374:CCEWAO>2.0.CO;2](https://doi.org/10.1175/1520-0469(1999)056<0374:CCEWAO>2.0.CO;2).
- , and H. H. Hendon, 2004: An all-season real-time multivariate MJO index: Development of an index for monitoring and prediction. *Mon. Wea. Rev.*, **132**, 1917–1932, doi:[10.1175/1520-0493\(2004\)132<1917:AARMMI>2.0.CO;2](https://doi.org/10.1175/1520-0493(2004)132<1917:AARMMI>2.0.CO;2).
- Yoo, C., S. Lee, and S. B. Feldstein, 2012a: Arctic response to an MJO-like tropical heating in an idealized GCM. *J. Atmos. Sci.*, **69**, 2379–2393, doi:[10.1175/JAS-D-11-0261.1](https://doi.org/10.1175/JAS-D-11-0261.1).
- , —, and —, 2012b: Mechanisms of Arctic surface air temperature change in response to the Madden–Julian oscillation. *J. Climate*, **25**, 5777–5790, doi:[10.1175/JCLI-D-11-00566.1](https://doi.org/10.1175/JCLI-D-11-00566.1).
- , S. B. Feldstein, and S. Lee, 2014: The prominence of a tropical convective signal in the wintertime Arctic temperature. *Atmos. Sci. Lett.*, **15**, 7–12, doi:[10.1002/asl2.455](https://doi.org/10.1002/asl2.455).
- Zhang, C., 2005: Madden-Julian oscillation. *Rev. Geophys.*, **43**, RG2003, doi:[10.1029/2004RG000158](https://doi.org/10.1029/2004RG000158).
- , M. Dong, S. Gualdi, H. H. Hendon, E. D. Maloney, A. Marshall, K. R. Sperber, and W. Wang, 2006: Simulations of the Madden-Julian oscillation in four pairs of coupled and uncoupled global models. *Climate Dyn.*, **27**, 573–592, doi:[10.1007/s00382-006-0148-2](https://doi.org/10.1007/s00382-006-0148-2).